

3-Substituted Indole Inhibitors Against *Francisella tularensis* FabI Identified by Structure-Based Virtual Screening

Xin Hu,^{§,#} Jaimee R. Compton,^{†,‡,#} Mohamed Diwan M. AbdulHameed,[⊥] Charles L. Marchand,^{||} Kelly L. Robertson,[†] Dagmar H. Leary,[†] Ajit Jadhav,[§] Jeremy R. Hershfield,^{||} Anders Wallqvist,[⊥] Arthur M. Friedlander,^{||} and Patricia M. Legler^{*,†}

[†]Center of Bio/Molecular Science and Engineering, Naval Research Laboratories, Washington, D.C. 20375, United States

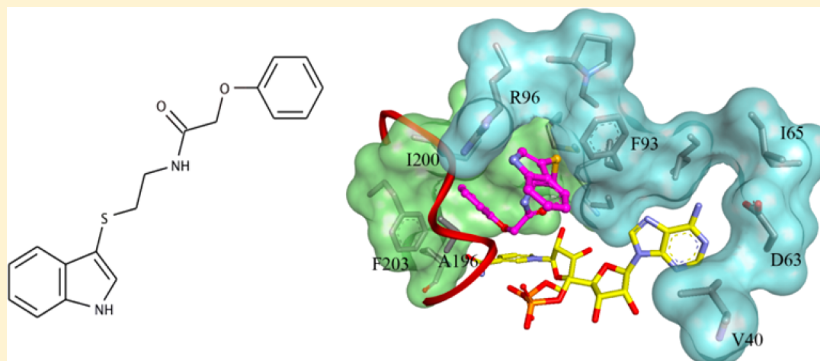
[‡]Nova Research, Inc., Alexandria, Virginia 22308, United States

[§]NIH Chemical Genomics Center, National Center for Advancing Translational Sciences, Rockville, Maryland 20850, United States

^{||}U.S. Army Medical Research Institute of Infectious Diseases, Frederick, Maryland 21702-5012, United States

[⊥]Biotechnology HPC Software Applications Institute, Telemedicine and Advanced Technology Research Center, U.S. Army Medical Research and Materiel Command, Fort Detrick, Maryland 21702, United States

S Supporting Information



ABSTRACT: In this study, we describe novel inhibitors against *Francisella tularensis* SchuS4 FabI identified from structure-based in silico screening with integrated molecular dynamics simulations to account for induced fit of a flexible loop crucial for inhibitor binding. Two 3-substituted indoles, **54** and **57**, preferentially bound the NAD⁺ form of the enzyme and inhibited growth of *F. tularensis* SchuS4 at concentrations near that of their measured K_i . While **57** was species-specific, **54** showed a broader spectrum of growth inhibition against *F. tularensis*, *Bacillus anthracis*, and *Staphylococcus aureus*. Binding interaction analysis in conjunction with site-directed mutagenesis revealed key residues and elements that contribute to inhibitor binding and species specificity. Mutation of Arg-96, a poorly conserved residue opposite the loop, was unexpectedly found to enhance inhibitor binding in the R96G and R96M variants. This residue may affect the stability and closure of the flexible loop to enhance inhibitor (or substrate) binding.

■ INTRODUCTION

Francisella tularensis is a facultative intracellular Gram-negative bacterium responsible for the disease tularemia. *F. tularensis* is classified as a tier 1 Select Agent as it could potentially be used as a biological weapon. It can incapacitate or cause death with doses as small as 25 colony-forming units.¹ Without treatment, the mortality rate can be as high as 5–15% for type A strains and 30–60% for the severe systemic and pneumonic forms of the disease.² Of the antibiotics that have been proven to be effective, streptomycin was historically the preferred treatment for tularemia.^{1,3} However, it and other aminoglycosides such as gentamicin have been associated with ototoxicity (irreversible cochlear and vestibular damage)⁴ and nephrotoxicity⁵ and require parenteral administration.^{3,6,7} While ciprofloxacin is an easily administered oral antibiotic effective against experimental

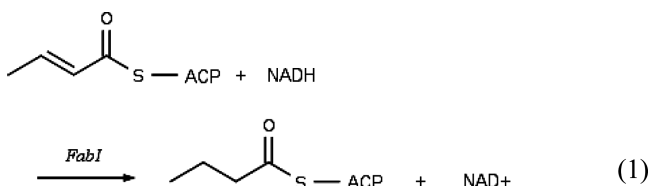
infections with *F. tularensis* SchuS4,⁸ resistance to ciprofloxacin can arise from single-point mutations within a region of DNA gyrase known as the quinolone resistance-determining region (QRDR).^{9,10} Ciprofloxacin-resistant strains of *F. tularensis*,¹¹ *Bacillus anthracis*,¹² *Yersinia pestis*,¹³ *Escherichia coli*,^{9,14} and *Streptococcus pneumoniae*^{15,16} are well documented,¹¹ and ciprofloxacin resistance in *E. coli* and *Pseudomonas aeruginosa* is now $\geq 40\%$.^{17,18} Thus, there continues to be a need to identify new drugs effective against tularemia that are safe and practical to administer.

The viability of *F. tularensis*, as well as that of a variety of other Gram-negative and Gram-positive bacteria such as *E. coli*,

Received: January 2, 2013

Published: July 1, 2013

Staphylococcus aureus, and *Bacillus subtilis*, is highly dependent upon its type II fatty acid synthesis pathway (FAS II). The FAS II pathway differs distinctly from the mammalian type I multienzyme fatty acid synthase (FAS I) making the multifunctional enzyme components of the FAS II pathway ideal targets for selective inhibition. FabI, a NADH-dependent enoyl acyl carrier protein reductase (ENR) (EC 1.3.1.9), serves to catalyze the final reaction in the chain elongation cycle (eq 1).^{19,20} However, at least three other ENR isozymes, FabK,



FabL, and FabV, can catalyze the same reaction as FabI in fatty acid biosynthesis.^{21–23} FabK²² is structurally unrelated to FabI, FabL, and FabV and is resistant to triclosan;²⁴ its presence can thereby confer triclosan resistance. FabL and FabV are structurally similar to FabI, but share low sequence identity and are poorly inhibited by triclosan.^{25,26} *S. pneumoniae* and *P. aeruginosa* contain FabK,²⁴ and *Vibrio cholerae*,²⁷ *P. aeruginosa*,²⁸ *Y. pestis*,²⁹ and *Burkholderia mallei*³⁰ contain FabV. FabI is the sole ENR in *F. tularensis*, *B. anthracis*, *E. coli*, and *S. aureus*. Because *F. tularensis* and *S. aureus* FabI are essential for lipid biosynthesis even in the presence of exogenous lipids,^{31–33} FabI is an attractive target for antimicrobial drug design.³⁴

Triclosan, diazaborines, and the frontline antituberculosis drug, isoniazid, have all been shown to inhibit ENRs. Triclosan, the most well-known of these inhibitors, is a biphenyl ether that has been used ubiquitously as an antimicrobial additive in hand soap, toothpastes, mouth rinses, and other such consumer products (in the range of 0.1–0.3% of product weight) for over 25 years.^{35–37} However, a variety of adducts (glucose, mercapturic acid, and cysteine conjugates) form with the biphenyl rings in vivo and the compound is rapidly cleared from the blood and excreted in the urine, making it ineffective as an oral antibiotic.³⁸ While several species-specific FabI inhibitors have been identified,³⁹ broad spectrum inhibition of FabI enzymes has been particularly difficult. Structurally, FabI contains a characteristic and mostly conserved substrate binding site which is shielded by a highly flexible loop (residues 192–205 in *F. tularensis* FabI).^{26,40} Triclosan preferentially binds the NAD⁺ product complex, and the loop is found clamped down in a closed form.⁴¹ Because triclosan inhibition of FabI exhibits slow-onset kinetics, indicative of the ordering of the substrate binding loop, it is believed that the loop

stabilization upon inhibitor binding is a key determinant of binding affinity and selectivity.^{19,41–43}

Structure-based virtual screening has been successfully applied to the identification of small molecule inhibitors against specific targets. For pathogens which require BSL3/4 environments, high throughput screening of chemical libraries using cell-based assays is not typically practical, thus computational methods in combination with in vitro assays offer an appealing alternative to antimicrobial drug discovery. The X-ray crystal structures of FabI, free and bound to triclosan, have recently been determined.^{19,44,45} Insights into the binding interaction of triclosan in the active site and dynamic properties associated with the flexible substrate binding loop allowed us to carry out structure-based in silico screening to search large-scale databases for novel inhibitors against FabI. The combination of molecular dynamics with docking protocols has been proposed to be more effective than molecular docking alone,⁴⁶ but must be optimized for screening particular target proteins. Herein we describe the use of a combination of in silico high throughput screening, modeling, and kinetic analyses to identify inhibitors of *F. tularensis* FabI with novel chemotypes.

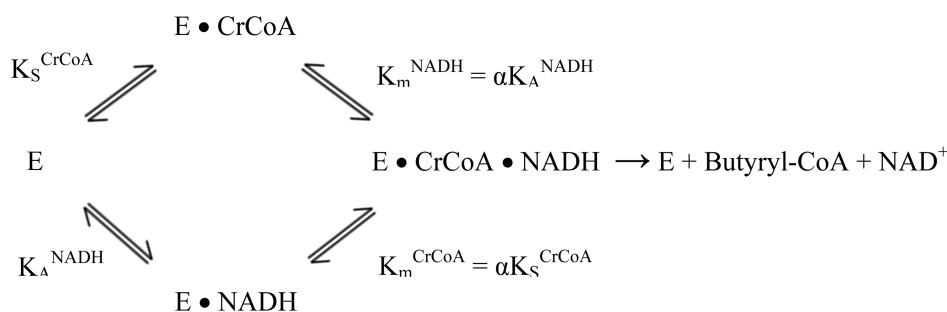
METHODS

Reagents. All buffers, substrates, and solvents were purchased from Sigma (St. Louis, MO). Ciprofloxacin was purchased from the U.S. Pharmacopeia as a certified reference standard, 100.0% pure (Rockville, MD). All compounds were purchased from ChemNavigator. Purity was determined by LC-ESI-MS by analyzing the HPLC chromatograms, masses, and isotopic distributions. Inhibitors **41**, **54**, and **57** were 86, 84.5, and >99% pure, respectively, and were from the Aldrich Market Select screening compound collection (¹H NMR and mass spectra are provided in the Supporting Information).

Protein Purification and Expression. The pet23b expression plasmid carrying FtufabI with a C-terminal His₆-tag was synthesized by Genscript, Inc. (Piscataway, NJ). The plasmid was transformed into BL-21 (DE3) pLysS *E. coli* (Novagen). The cells were grown at 37 °C until reaching an OD₆₀₀ of 0.8–1.0 before induction with 0.2 mM IPTG. The cells were harvested after an overnight induction period at 17 °C. The cells were lysed and sonicated and loaded onto a nickel-charged Chelating Sepharose column (GE Healthcare) equilibrated with buffer containing 20 mM Tris pH 7.6 and 500 mM NaCl. For the mutants, 5% glycerol was added to the buffers. The column was washed with buffer containing 60 mM imidazole, and the protein was eluted with buffer containing 300 mM imidazole. The protein was further purified using a Superdex G-75 column (GE Healthcare) equilibrated with 30 mM PIPES pH 8.0, 150 mM NaCl, and 1 mM EDTA. Protein concentration was determined using a calculated extinction coefficient of $\epsilon_{280} = 17,670 \text{ mM}^{-1} \text{ cm}^{-1}$ and a molecular weight of 28,870 Da.

In Vitro Assays. Two methods of detection, fluorescence and UV–vis, were used to monitor the oxidation of NADH to NAD⁺.^{19,47}

Scheme 1. Thermodynamic Box for Ternary Complex Formation



Single point enzyme assays included 160 μM crotonyl CoA (CrCoA), 250 μM NADH, ± 200 μM NAD⁺, 20 μM of inhibitor (or DMSO for control reactions) in 30 mM PIPES, pH 8.0, 150 mM NaCl. Rates were measured at 37 °C by monitoring the absorbance of NADH by UV-vis (340 nm). IC₅₀ values for the 140 compounds were measured at 23 \pm 3 °C by monitoring the fluorescence of NADH (ex = 360 nm, em = 425 nm) in the same buffer. The IC₅₀ for triclosan and inhibitors 41, 54, and 57 were determined using 160 μM CrCoA (for WT) or 1 mM CrCoA (for variants), 200 μM NAD⁺, 250 μM NADH, and varying concentrations of inhibitor (0–2 mM). Wells with heavy or visible compound precipitation were excluded from data analysis. The reaction was initiated with enzyme (4 nM of WT or 0.12 μM of the variants), and data was collected at 340 nm (UV-vis) at room temperature (23 \pm 3 °C).

Steady State Kinetics of FabI and its Variants. Steady state kinetic parameters were measured by monitoring the change in absorbance at 340 nm. Initial velocities were measured with varying CrCoA and NADH concentrations in 30 mM PIPES pH 8.0, 150 mM NaCl, at room temperature (23 \pm 3 °C). Data was globally fit to a velocity equation for a bisubstrate system with ternary complex formation (random order) using Grafit 6.0 (Erithacus Software Limited). K_A' is the dissociation constant for the binary EA complex, and K_A and K_B are the Michaelis constants for substrates A and B, respectively (Scheme 1).

$$v = \frac{V_{\max}[A][B]}{K_A'K_B + K_B[A] + K_A[B] + [A][B]} \quad (2)$$

Effect of NAD⁺ on K_i' . To determine if the inhibitors selectively bound the NAD⁺ complex apparent inhibition constants, K_i' , were measured using a saturating concentration (200–333 μM) of NAD⁺. FtuFabI (160 nM) was added to NAD⁺, NADH (12.5–500 μM), and inhibitor (2.5–12 μM). The reactions were initiated with CrCoA (160 μM) and monitored at 340 nm for 5 min.

Testing of FabI Inhibitors on Growth of *Francisella tularensis* and *Bacillus anthracis*. Minimum inhibitory concentrations (MICs) were determined by the microdilution method in 96-well plates according to Clinical Laboratory Standards Institute guidelines.⁴⁸ *Escherichia coli* (ATCC25922), *Pseudomonas aeruginosa* (ATCC 27853), or *Staphylococcus aureus* (ATCC 29213) were used for internal quality control. *F. tularensis* (SchuS4) and *B. anthracis* (Ames) were from the U.S. Army Medical Research Institute of Infectious Diseases collection.

FabI inhibitors were dissolved in DMSO (Sigma-Aldrich, St. Louis, MO). Ciprofloxacin was used as a comparator antibiotic. The inhibitors and comparator were thawed and immediately diluted 1:20 into freshly prepared Cation-Adjusted Mueller–Hinton Broth (CAMHB) (Becton Dickinson, Franklin Lakes, NJ) to generate working stocks. Then 50 μL of the FabI inhibitor or comparator antibiotic working stock solutions were placed into wells of the first column of a 96-well plate and serially diluted in CAMHB. To these wells, 50 μL of freshly prepared bacterial inocula were added. DMSO without inhibitor was used for comparison and showed no inhibitory activity against any of the bacteria tested.

Bacterial inocula were prepared by serial passage (twice) and incubation at 35 \pm 2 °C on agar plates using starting samples removed from freezer stocks of each strain. Chocolate agar was used for *F. tularensis* and sheep blood agar for *B. anthracis*, *E. coli*, *P. aeruginosa*, and *S. aureus*. Colonies were taken from the second passage plate and suspended, with gentle vortexing, into CAMHB for *B. anthracis*, *E. coli*, *P. aeruginosa*, and *S. aureus*, or CAMHB+4%IsoVitalX (Becton Dickinson) for *F. tularensis*. Suspended cultures were diluted with CAMHB (+4%IsoVitalX for *F. tularensis*) to the desired bacterial cell density based on OD₆₀₀. Following the addition of 50 μL of the diluted bacterial inocula to each well containing serially diluted FabI inhibitor (at 50 μL volume), the resulting final bacterial concentration was approximately 5 \times 10⁴ CFU/mL.

Plates were incubated in air at 35 \pm 2 °C. MICs (first well with no visible growth) were determined visually at 18–24 h for *B. anthracis*, *E. coli*, *P. aeruginosa*, and *S. aureus* or 42–48 h for *F. tularensis*. The

antibiotic or inhibitor ranges covered were 8–0.004 $\mu\text{g}/\text{mL}$ (ciprofloxacin), 52–0.26 $\mu\text{g}/\text{mL}$ (compound 41), 343–0.17 $\mu\text{g}/\text{mL}$ (compound 54), and 413–0.202 $\mu\text{g}/\text{mL}$ (compound 57).

Cytotoxicity Assays. 786-O (ATCC CRL-1932), a human renal cell adenocarcinoma line, and Neuro-2a (ATCC CCL-131), a mouse neuronal line, were maintained in Eagle's Minimum Essential Medium and RPMI-1640 medium, respectively, both supplemented with 10% fetal bovine serum and penicillin/streptomycin (50 units/mL, 50 $\mu\text{g}/\text{mL}$). The day before compound addition, 10³ cells/well were plated in 96-well plates in their respective media and incubated overnight at 37 °C under 5% CO₂. The next day, the test compounds were added after making 2-fold serial dilutions in DMSO. The concentrations of the compounds were dependent on their solubility in DMSO, and an equivalent amount of DMSO was added to control wells. Following compound addition in triplicate, cells were incubated at 37 °C under 5% CO₂ for 72 h. The cells were then washed with PBS and CellTiter 96 Aqueous One solution was added to each well and the plates were incubated for 2 h at 37 °C. The absorbance at 490 nm was read, and percent survival (relative to the DMSO control) was used to determine the 50% lethal concentration (LC₅₀) using GraFit 6.0.1 software (Erithacus Software Limited).

Modeling of FabI–NAD–Triclosan Binding Complex. The three-dimensional structure of FabI from *F. tularensis* was obtained from the Protein Data Bank (PDB code 2JJY).⁴⁹ The structure is a tetramer in complex with the cofactor, NAD, bound in the active site. However, the substrate-binding loop (192–205) is disordered in the crystal structure. Experimental studies have shown that triclosan (TCL) is a slow-onset inhibitor that induces conformational changes in the loop and stabilizes the inhibitor in a closed form in the inhibitor-bound complex.⁴⁵ Therefore, we modeled the substrate binding loop of FtuFabI in the presence of the NAD cofactor and triclosan and generated the A monomer (Supporting Information Figure S1). The NAD complex was extracted, and all water molecules were removed. The substrate-binding loop was constructed using the program Modeler⁵⁰ with a homologue template of FabI from *E. coli* in complex with triclosan (PDB 1QSG,⁴⁵ identity 57%). The binding complex of FtuFabI–NAD–TCL was energy-minimized using the AMBER 11 package. The refined structural model of FtuFabI in the presence of NAD was used for the following in silico screening.

Virtual Screening: Round I. The AutoDock-based DOVIS program^{51,52} was used to screen the NIH Molecular Library Small Molecule Repository (MLSMR) collection of ~350000 compounds against the structure model of FtuFabI–NAD. The active site of the protein was defined by a grid of 60 \times 60 \times 60 points with a grid spacing of 0.35 Å centered at the center of mass of NAD. The Lamarckian Genetic Algorithm (LGA) was used with 50 runs, and clustering of docked poses was applied according to the RMSD. The best pose with lowest AutoDock score of the top three clusters were retained for each compound. The predicted binding poses of the entire database were ranked by AutoDock score overall, and the top 20000 compounds were extracted. Two steps of postprocessing were utilized for hit selection. First, the retrieved 20000 compounds were energy-minimized in the binding site of FabI followed by rescoring with three different scoring functions (AutoDock 4.0, LigScore 2, and X-SCORE). The top 500 compounds from each score list were pooled, and duplicates were removed. Second, the resulting unique compounds (~1000 compounds) were subjected to a short MD simulation (100 ps) in implicit solvent, and the binding free energies were calculated with the MM-PBSA method. Finally, the top-ranked 200 hits were visually inspected and 75 commercially available compounds were cherry picked for experimental evaluation.

Virtual Screening: Round II. A recent X-ray crystal structure of FabI from *F. tularensis* (FtuFabI) bound to NAD⁺ and triclosan (PDB code 3NRC)⁴⁴ was reported after the start of round I virtual screening. The complete structure of FtuFabI including the structured substrate binding loop was determined in this crystal structure. In an effort to identify FabI inhibitors with new scaffolds, we carried out a second round of virtual screening using PDB 3NRC. The ChemNavigator database contains ~14 million unique compounds and was screened using the 2D similarity search option in Pipeline Pilot. Six known FabI

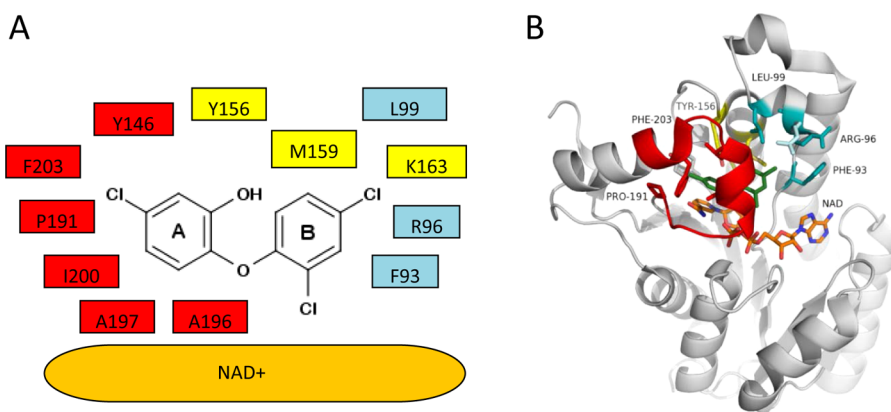


Figure 1. Binding interactions of FtufabI with triclosan and NAD⁺. (A) The residues are colored according to their “binding nature,” the same residues are shown in the structure (PDB 3NRC⁴⁴) shown in (B). Residues belonging to the flexible substrate-binding loop become ordered upon inhibitor binding and are colored red; electron density for these residues is not observed in the absence of inhibitor (PDB 2JJY¹⁹). Yellow residues are part of the conserved catalytic site. In blue are residues at the rim of the binding pocket which may affect loop closure and are variable among bacterial species. Arg-96 can be found in two conformations in the free (light blue, PDB 2JJY) and triclosan-bound (darker blue, PDB 3NRC) structures. The oxidized cofactor, NAD⁺, is colored in orange and provides additional binding interactions with the inhibitor. Figure was prepared with Pymol (DeLano Scientific LLC, San Carlos, CA, USA).

inhibitors that were cocrystallized with other FabI were collected and used as query molecules. The molecules were obtained from PDBs 2OPO (*P. falciparum*),⁵³ 3OIG (*B. subtilis*),⁵⁴ 1I2Z (*E. coli*),⁵⁵ 1LX6 (*E. coli*),⁵⁶ 1LXC (*E. coli*),⁵⁶ and 1MFP (*E. coli*)⁵⁷ (Supporting Information Figure S2). The top 2000 most similar molecules were selected and subjected to hierarchical virtual screening protocol in the Glide program.^{34–36} In addition, 1150 approved drugs from the DrugBank⁵⁸ were screened using a similar protocol, combined Glide XP docking and a 3D-ligand based similarity search program, ROCS.⁵⁹ Finally, the top-ranked 200 hits were visually inspected and 65 commercially available compounds were selected for experimental evaluation.

MD Simulations and Binding Free Energy Calculations. MD simulations were conducted for the optimized binding mode of inhibitors with FabI in explicit solvent using the AMBER 11 package and the ff99SB force field.⁶⁰ The solvated protein systems were subjected to a thorough energy minimization prior to MD simulations by first minimizing the water molecules while holding the solute frozen (1000 steps using the steepest descent algorithm), followed by 5000 steps of conjugate gradient minimization of the whole system to remove close contacts and to relax the system. A nonbonded cutoff of 10 Å was used, and the nonbonded pair list was updated every 25 time steps. Periodic boundary conditions were applied to simulate a continuous system. The particle mesh Ewald (PME) method was employed to calculate the long-range electrostatic interactions.⁶¹ The simulated system was first subjected to a gradual temperature increase from 0 to 300 K over 100 ps and then equilibrated for 500 ps at 300 K, followed by production runs. Constant temperature and pressure (300 K/1 atm) were maintained using the Berendsen coupling algorithm⁶² with a time constant for heat-bath coupling of 0.2 ps.

The binding free energies were calculated using the MM-PBSA method.⁶³ A set of 100 snapshots was extracted from trajectories of binding complexes at 10 ps intervals from the 2 ns of each MD simulation. The polar contribution (G_{PB}) was calculated using the Poisson–Boltzmann equation. The nonpolar contributions (G_{SA}) were estimated using the MSMS algorithm according to the equation: $G_{SA} = \gamma \times \text{SASA} + b$ kcal/mol, with γ and b set to 0.00542 kcal/mol·Å² and 0.92 kcal/mol, respectively, and the probe radius used to calculate the solvent accessible surface area (SASA) was set to 1.4 Å. The entropy contribution was neglected in the binding free energy calculation. Binding free energy decomposition was performed using the same MM-PBSA module in AMBER 11 package.

RESULTS AND DISCUSSION

Structural Features of Inhibitor Binding with FabI.

Structures of FabI in the apo and inhibitor-bound states have been studied in various bacterial species.^{23,41,44,45,64–67} A comparative analysis of the binding interactions of triclosan with FabI enzymes from seven different species revealed key residues and essential structural elements for inhibitor binding (Supporting Information Figure S1). As shown in the FtufabI–NAD⁺–triclosan complex (PDB 3NRC⁴⁴) (Figure 1), the planar aromatic ring of triclosan carrying the hydroxyl group binds in the interior of the pocket (A-ring binding site) and makes a π – π interaction with the nicotinamide group of the NAD cofactor. While the 5-chlorophenyl group points toward Pro-191 and forms stacking interactions with Tyr-146 and Phe-203, the hydroxyl group forms a hydrogen-bond with the side chain of residue Tyr-156, which is essential for the activity of triclosan.^{36,41,44,68–70} Residues from the flexible loop including Ala-197, Ile-200, and Phe-203 form the wall of the hydrophobic pocket, and structure-based sequence alignment showed that these residues are mostly conserved (Supporting Information Figure S1). On the other hand, the dichlorophenyl ring of triclosan is orientated toward the hydrophobic entrance of the pocket (B-ring binding site). This region mainly consists of residues Phe-93, Leu-99, Lys-163, Tyr-156, and Met-159, which are also typically conserved among species. Arg-96 is located at the top of the entrance of the B-ring binding site opposite of the substrate binding loop but is poorly conserved. In addition, the oxidized cofactor NAD⁺ makes significant contributions to the inhibitory activity of triclosan by forming extensive interactions with both the A and the B rings of triclosan.

Structural Model of FtufabI. The substrate binding loop of FabI, which is disordered in the structure 2JJY,¹⁹ was modeled with the cofactor and triclosan using EcFabI as a template (1QSG⁴⁵) (Supporting Information Figure S1). The FtufabI–NAD⁺–triclosan complex was further refined with MD simulations. Compared to the later released crystal structure 3NRC,⁴⁴ which has complete coordinates for the loop residues and was used in the second round of screening, the refined structural model of FtufabI showed the same 3D

fold and active site residue conformations (RMSD = 0.79 Å over 256 C_{α} , Supporting Information Figure S1). While small differences were observed, triclosan interacted with the substrate binding loop in a similar manner in both the modeled structure and crystal structure. A notable difference was found in the side chain of Arg-96, which pointed downward, whereas the side chain was oriented away from the loop in the triclosan-bound crystal structure (3NRC).⁴⁴ In 3NRC, R96 had higher B -factor values suggesting static or dynamic disorder of the side chain. The role of Arg-96 in inhibitor and substrate binding is discussed below.

Virtual Screening Hits. We performed two rounds of virtual screening using structural and ligand-based approaches to search the MLSMR and ChemNavigator databases (Figure 2). Structure-based docking was performed in the first round

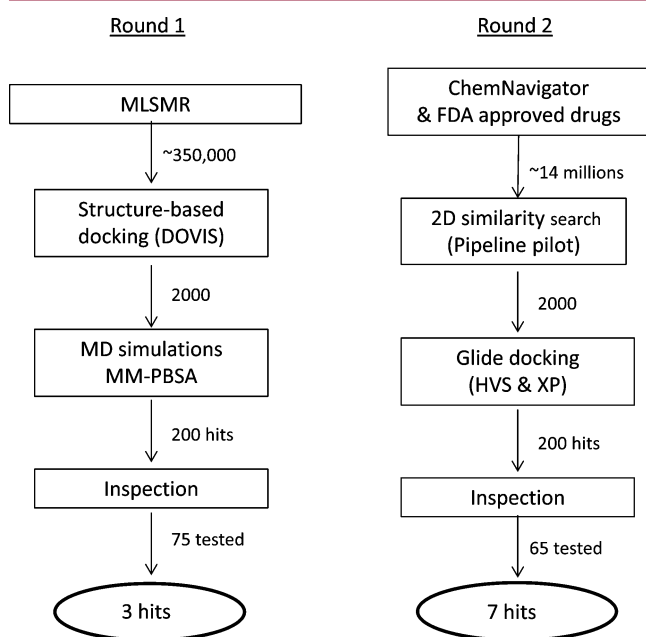


Figure 2. Summary of VS strategies used in the two rounds of screening.

screen for the MLSMR library (~340000 unique compounds) using the structural model of FabI, followed by MD simulations and MM-PBSA calculation of top hits in the postprocessing for hit selection. The second screen was performed using a fast 2D-similarity searching method for the large ChemNavigator database (over 14 million compounds). The top hits were prioritized with a hierarchical docking approach. For drug-repurposing, a small library of FDA approved drugs was also screened. The results of identified hits were summarized in Figure 3 and Supporting Information Figure S2.

The three most potent hits with low micromolar inhibitory activity, inhibitors **41**, **54**, and **57**, were identified from the first-round of screening. The measured K_i values were K_i (**41**) = 7 ± 2 μ M, K_i (**54**) = 3.4 ± 0.7 , and K_i (**57**) = 12 ± 3 μ M. Compound **41** is a phenyl oxadiazole derivative with a sulfonyl-pyrrolidine group, whereas **57** and **54** contain a 3-substituted indole group. An N -methyl indole inhibitor identified at GSK was shown to have inhibitory activity against *S. aureus*, *H. influenzae*, and *S. pneumoniae*⁷¹ (Supporting Information Figure S3). The *F. tularensis* FabI inhibitors identified by Hevener et al. contain a structurally similar benzimidazole group (Supporting Information Figure S3).⁵² In comparison, our 3-substituted

indole inhibitors appear to possess a distinct scaffold that differs from these known FabI inhibitors. Surprisingly, no interesting hits were identified from the second round of screening using a similarity search. These hits were generally weak binding inhibitors (IC_{50} 47–79 μ M) and not suitable for antimicrobial activity. We believe that the robust performance of the first-round of screening was gained from the MD simulations in combination with MM-PBSA scoring. This approach has been applied to drug discovery with various targets to account for protein flexibility and inhibitor-induced fit.⁴⁶ These effects are especially relevant to the binding of FabI inhibitors because the flexible substrate-binding loop is known to undergo conformational changes which stabilize inhibitor binding in the closed form (Figure 1, Supporting Information Figure S1).^{41,42,45}

Binding Mode Analysis. The binding interactions of the three identified inhibitors to FabI (**41**, **54**, and **57**) were further investigated with MD stimulations and binding free energy calculations. Similar to triclosan and other known inhibitors observed in cocrystal structures, these small molecule inhibitors were well accommodated in the active site of FabI. The inhibitors made interactions with mostly conserved residues in the A- and B-ring binding pockets (Figure 4). An interesting finding is that the two indole-based inhibitors adopted different binding conformations. The indole group of **57** was found to occupy the interior of the A-ring binding pocket, forming a stacking interaction with Tyr-146, Phe-203, and the nicotinamide group of NAD, whereas **54** adopted a binding conformation with the indole pointed outward to the B-ring binding site and made extensive interactions with Phe-93 as well as residues in the flexible loop 192–205. MD stimulations indicated that the binding complex remained stable while the loop was significantly stabilized. The calculated binding free energies of the three inhibitors were in agreement with experiments of measured K_i (Supporting Information Figure S4 and S5).

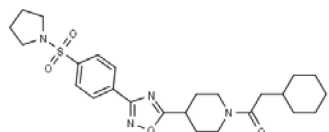
Further binding free energy decomposition revealed more details of key residues that contributed to the binding interactions (Figure 4). Tyr-146 had the largest contributions to the binding free energies of all three inhibitors, reiterating the importance of this H-bonding interaction commonly found with known FabI inhibitors. Tyr-156 and Met-159 in the interior of the binding pocket also played an important role in inhibitor binding by forming extensive π -stacking and hydrophobic interactions. Remarkably, residue Phe-93 had the largest binding energy contributions to inhibitors **41** and **57** at the B-ring binding site, while the loop residues such as Ala-197 and Phe-203 contributed greatly to inhibitor **54** binding. These predictions were utilized to select several of the site-directed mutants for kinetic analysis.

Inhibitors Preferentially Bind the E–NAD⁺ Complex.

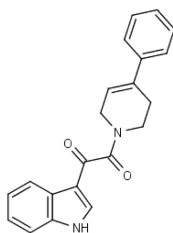
Triclosan specifically binds the NAD⁺ bound form of the enzyme in a slow-onset manner with the ordering of the substrate binding loop.⁴⁴ In *E. coli* FabI, the substrate binding loop has also been shown to become structured upon binding acyl carrier protein but in a slightly different conformation than that observed in the NAD⁺–triclosan complex.⁴¹ Because the in silico screening began with a modeled loop between residues 192–205 the impact of this model on the inhibitor binding specificity was not known for the compounds selected from the in silico screening, thus kinetic methods were employed to examine inhibition of the NADH-bound form and the NAD⁺-bound form.

Round I

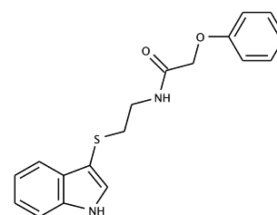
MLSMR



41 ($K_i = 7 \mu\text{M}$)



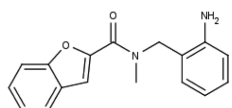
57 ($K_i = 12 \mu\text{M}$)



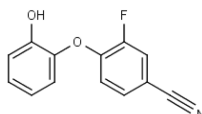
54 ($K_i = 3.4 \mu\text{M}$)

Round II

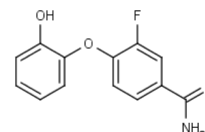
ChemNavigator



137 ($\text{IC}_{50} = 45 \mu\text{M}$)

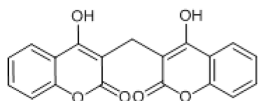


139 ($\text{IC}_{50} = 11 \mu\text{M}$)

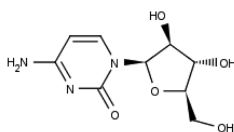


140 ($\text{IC}_{50} = 6 \mu\text{M}$)

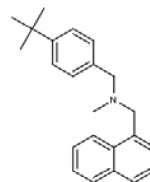
Approved Drugs



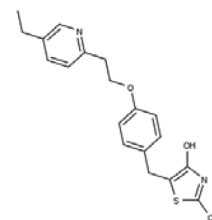
Dicumarol
($\text{IC}_{50} = 47 \mu\text{M}$)



Cytarabine
($\text{IC}_{50} = 59 \mu\text{M}$)



Butenafine
($\text{IC}_{50} = 76 \mu\text{M}$)



Pioglitazone
($\text{IC}_{50} = 79 \mu\text{M}$)

Figure 3. Structures of hits obtained through in silico screening.

The three inhibitors were found to be in rapid equilibrium and no evidence of slow-onset inhibition was apparent in progress curves (Supporting Information Figure S6). Inhibitor concentrations were varied in the presence or absence of NAD^+ and subplots of the slopes or intercepts versus inhibitor concentration revealed linear inhibition in the presence of NAD^+ , but not in its absence, consistent with inhibitor binding to a single form (E-NAD^+) of the enzyme at one site with complete inhibition (Figure 5 and Supporting Information Figure S7). Both inhibitors were linear competitive inhibitors with respect to the CrCoA substrate. Inhibitor binding was only detectable in the presence of NAD^+ but not in its absence (as evidenced by the relatively flat lines in the subplots of $[I]$ vs slope and $[I]$ vs intercept, Figure 5 and Supporting Information Figure S7). The inhibitors affected the slope (K_m/V_{max}) but not the intercept ($1/V_{\text{max}}$), consistent with competitive inhibition with respect to the CrCoA substrate (Table 2). The preferential binding of the inhibitors to the NAD^+ form versus the NADH -bound form also demonstrated specific binding and showed that the observed inhibition was not due to nonspecific effects such as denaturation, aggregation, unwanted side-reactions with substrates, or interference in the detection of product formation because the same inhibitor concentrations were tested in the presence and absence of NAD^+ . This result was also consistent

with the predicted contribution of the cofactor to the binding free energy (Figure 4).

Site-Directed Mutagenesis and Kinetic Analysis. On the basis of the predicted binding interactions and binding free energy analysis, seven variants (F93V, R96M, R96G, Y156F, M159T, A197M, and F203L) were constructed to examine the effects of these mutations on inhibitor binding using site-directed mutagenesis and kinetic analysis. To obtain the steady state kinetic parameters, initial velocities were measured and both CrCoA and NADH concentrations were varied in three-dimensional kinetic experiments (Supporting Information Figure S8). The data was globally fit to eq 2. In Lineweaver–Burk plots of $1/v$ vs $1/[\text{CrCoA}]$ and $1/v$ vs $1/[\text{NADH}]$, the lines converged indicating a sequential (ternary complex) mechanism rather than a substitution mechanism (ping-pong). In both plots, the lines converged on the abscissa, indicating that the binding of the first substrate had a small effect on the binding of the second (i.e., random-order ternary complex mechanism) (Supporting Information Figure S8). The formation of a ternary complex suggests direct transfer of the hydride to the substrate rather than to the enzyme (Supporting Information Figure S9). ENR with both types of kinetic mechanisms have been described in the literature.^{72–74} The

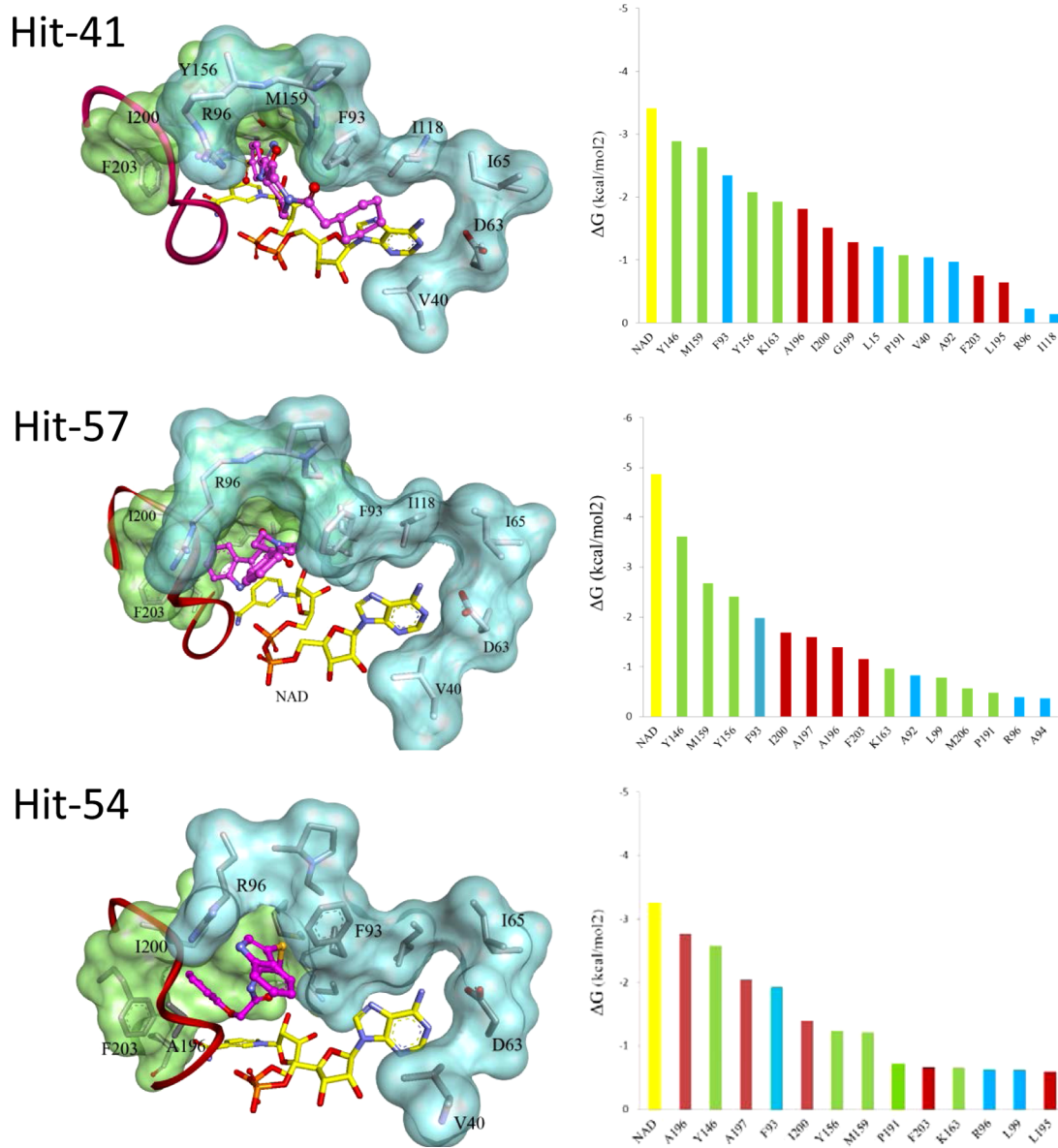


Figure 4. Binding interaction and binding free energy decomposition. Predicted binding interactions and binding free energy decomposition of hits 41, 54, and 57. The binding pockets of the active site of FabI are shown in surface representations (inner pocket in green and outer pocket in blue). The substrate-binding loop is shown as ribbon (red). Inhibitors bound in the active site are shown as sticks (carbon atom in magenta, oxygen in red, nitrogen in blue), and the cofactor NAD is colored yellow (carbon atom). Key residues contributing to the binding free energy are colored the same as their corresponding sub-binding pocket or loop. Figure was prepared with Pymol (DeLano Scientific LLC, San Carlos, CA, USA).

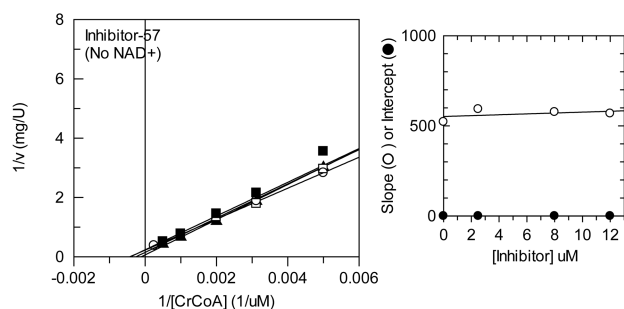
measured kinetic parameters for the WT enzyme are shown in Table 1.

Three of the selected variants (Y156F, M159T, and F203L) have been associated with triclosan resistance.^{36,37,75,76} Of the seven variants, only four had measurable activity, F93V, R96M, R96G, and F203L (Table 1). The F93V and F203L variants had significant reductions in activity (126–190-fold reduction in k_{cat}). The k_{cat} of the F93V variant was 190-fold lower than WT, however, no significant effect on the Michaelis constants for NADH and CrCoA was observed (<2-fold different), suggesting that F93 plays an important role in product release and/or catalysis. The F203L variant showed a similar decrease in activity (127-fold decrease) and no significant effect on the K_{m} (NADH) but a large 8-fold increase in the K_{m} (CrCoA), suggesting a role in substrate binding, catalysis, and/or product release. The locations of F93 and F203 are shown in Figure 1.

Phe-93 lies in the entrance of the substrate binding pocket, whereas the side-chain of Phe-203 is directed toward the interior of the pocket and is one of the substrate binding loop residues (residues 192–205).

The R96G and R96M mutations had an unusual effect. Arg-96 is present in FtufabI but is substituted by glycine in *E. coli* and *P. aeruginosa* and a methionine in *S. aureus*. Arg-96 is opposite of the flexible substrate-binding loop (Supporting Information Figure S1) and can be found in two different conformations in the triclosan-bound and free structures.^{19,44} In the WT, K_{m} approximately equals K_{s} , while in the mutants, $K_{\text{m}} < K_{\text{s}}$ (Table 1). A thermodynamic box relating the constants with a proportionality constant called α is shown in Scheme 1.⁷⁷ When $\alpha = 1$, the two sites are considered noninteracting; when $\alpha < 1$ or $\alpha > 1$, this indicates that the two sites interact (either tightening or weakening the binding of the second

A



B

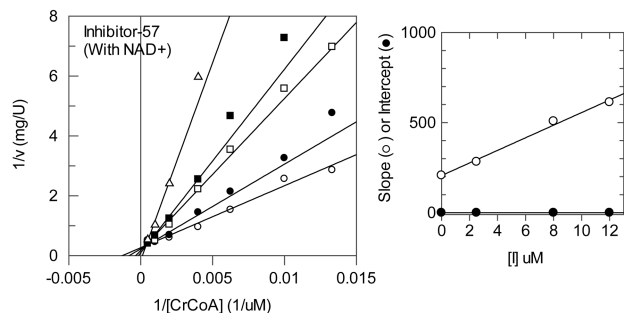


Figure 5. Effect of NAD^+ on inhibition. Inhibitors **41**, **54**, and **57** preferentially bind the NAD^+ -bound form of FtuFabI and are competitive inhibitors with respect to CrCoA. (A) Inhibition by inhibitor-57 with varying CrCoA in the presence of NAD^+ and (B) in the absence of NAD^+ . Subplots of the slope and intercept show that the inhibitor binding site is only titratable in the presence of NAD^+ consistent with the inhibitors forming E- NAD^+ -I ternary complexes. Data for other inhibitors can be found in the Supporting Information.

substrate). In the R96 variants, $\alpha < 1$ and binding of the first substrate led to tighter binding of the second. A significant reduction in the K_m (approximately 5-fold in R96 M and 10-fold in R96G) was observed (Table 1). Similar effects (i.e., tighter binding of inhibitors) were observed on the IC_{50} values. Therefore, interaction between the two sites may enable higher affinity substrate (or inhibitor) binding by stabilizing the flexible loop closure through either a new interaction or enhancement of an existing interaction.

Effects of Mutations on Inhibition. To determine if one or more of the identified chemotypes were affected by mutation, we measured the IC_{50} values of inhibitor **41**, **54**, **57**, and triclosan (Table 3). Of the three inhibitors, **57** showed the smallest increase (3-fold) in its IC_{50} value with the F93V variant. Both **41** and **54** showed significant increases (>14-fold and >6-fold increases, respectively) in the IC_{50} values when

Table 2. Kinetic Parameters of Inhibition

inhibitor	K_i (with NAD^+) with varying CrCoA (μM)	mode of inhibition with respect to CrCoA
41	7 ± 2	competitive
54	3.4 ± 0.7	competitive
57	12 ± 3	competitive

Table 3. Effects of Mutations on IC_{50} Values in the Presence of $200 \mu\text{M}$ NAD^+ without Pre-equilibration

enzyme	triclosan	41	54	57
FtuFabI WT	1.3 ± 0.2	8 ± 3	20 ± 5^a	3.0 ± 0.6
FtuFabI F93V	14 ± 5	>125	>125	9 ± 1
FtuFabI R96G	0.05 ± 0.02	0.8 ± 0.5	3 ± 2	0.3 ± 0.1
FtuFabI R96M	0.3 ± 0.1	0.17 ± 0.06	12 ± 6	0.6 ± 0.2
FtuFabI F203L	6.0 ± 0.8	5 ± 2	80 ± 20^a	14 ± 2

^aInaccurate due to poor solubility at higher concentrations.

measured with the F93V variant, and the IC_{50} values were >125 μM . Binding mode analysis showed that Phe-93 formed extensive vdW and aromatic stacking interactions and made significant binding free energy contributions to all three inhibitors (Figure 4). Notably, Phe-93 was predicted to make greater contributions to the binding free energies of **41** and **54** and a smaller contribution to **57**. Inhibitor **41** was not affected by the F203L variant, suggesting that this residue does not strongly contribute to its binding. In contrast, the IC_{50} values of **54** and **57** were found to increase by 4- and 5-fold, respectively. These results are consistent with the predicted binding mode and binding free energy analysis (Figure 4).

The effects of the Arg-96 mutations on inhibition were unexpected. The IC_{50} values for triclosan with the R96M and R96G variants were 4–26-fold lower. For inhibitor **41**, 10- and 45-fold decreases were observed for R96G and R96M, respectively. Similarly, 5- and 10-fold decreases were observed for inhibitor **57** with the R96M and R96G variants, respectively. The IC_{50} values for inhibitor **54** with the R96M and R96G variants were 1.7 and 6-fold lower, respectively. These results were rather surprising because the binding free energy analysis predicted that Arg-96 made only minor contributions. This suggested that the mutations enhanced or created new interactions with the inhibitor in some other manner. The importance of loop closure to substrate binding was previously demonstrated by mutation of the loop residue, Lys-201 to Glu, in *E. coli* FabI, which abolished activity.⁴¹ Arg-96 is located opposite to the substrate binding loop at the exterior of the binding site and could alter the loop flexibility and closure, consequently affecting inhibitor binding (Supporting Information Figure S1).

Table 1. Kinetic Parameters for FtuFabI and Its Variants at 22 ± 3 °C, pH 8.0

enzyme	K_A^{NADH} (mM)	K_S^{CrCoA} (mM)	K_m^{NADH} (mM)	K_m^{CrCoA} (mM)	k_{cat} (min^{-1})
WT	0.14 ± 0.04	0.24 ± 0.06	1.1 ± 0.3	1.8 ± 0.4	380 ± 60
F93V	0.6 ± 0.1	0.46 ± 0.08	2.1 ± 0.3	1.5 ± 0.4	2.0 ± 0.2
R96G	0.7 ± 0.1	0.08 ± 0.01	7 ± 1	0.7 ± 0.2	330 ± 30
R96M	0.6 ± 0.1	0.12 ± 0.04	1.6 ± 0.4	0.38 ± 0.09	240 ± 20
Y156F	ND				^a
M159T	ND				^a
A197M	ND				^a
F203L	1.0 ± 0.2	0.2 ± 0.1	9 ± 3	15 ± 8	3.0 ± 0.4

^aValues near limit of detection.

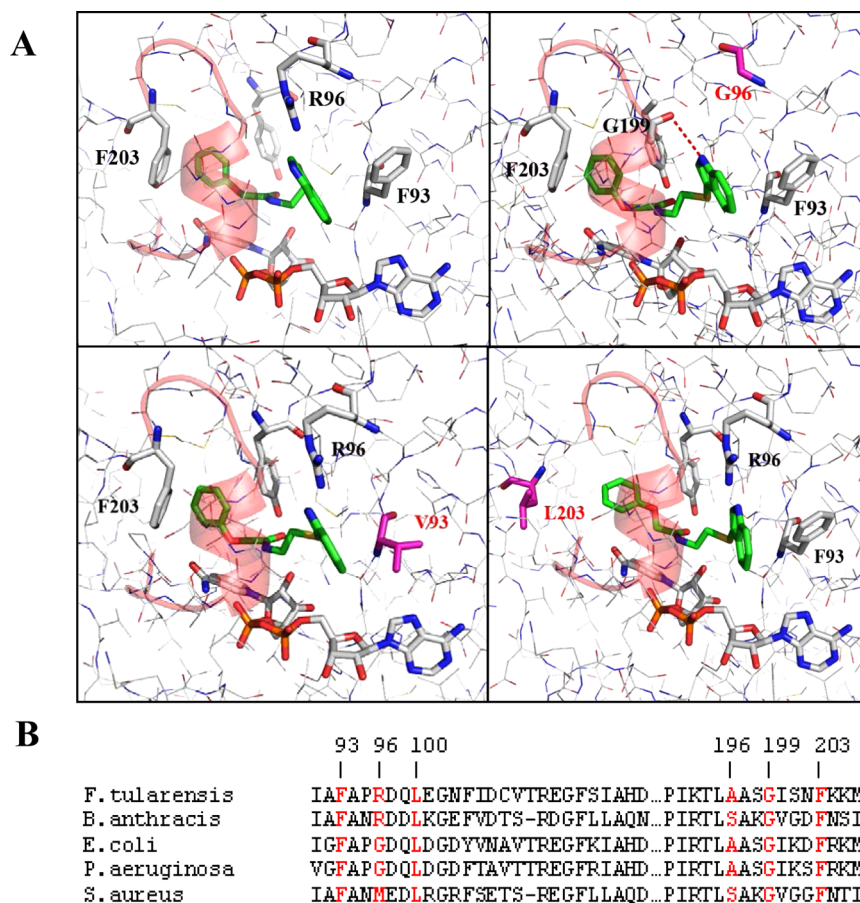


Figure 6. (A) Predicted binding interactions of inhibitor 54 with WT FtufabI and its variants, (B) Partial sequence alignment of FabI enzymes. Figure was prepared with Pymol (DeLano Scientific LLC, San Carlos, CA, USA).

To investigate this hypothesis, we examined the loop dynamics of the R96M and R96G variants in comparison with the wild-type using MD simulations and binding free energy calculations (Supporting Information Figure S10). The loop of the wild-type FabI in the apo state remained stable in a closed form during the time course of MD simulations, whereas it became more dynamic in the R96G and R96M variants. The more flexible loop may better accommodate the inhibitor (or substrate).⁴² Additionally, binding mode analysis showed that the indole group of inhibitor 54 could now interact with the substrate binding loop residue, Gly-199, through a new hydrogen bonding interaction, potentially altering the loop mobility in the inhibitor-bound state (Figure 6).

Cytotoxicity of Inhibitors. The cytotoxicity of inhibitors was determined using a colorimetric cell proliferation assay to measure cell survival in two cell lines, 786-O (human kidney) and Neuro2a (mouse neuronal) (Table 4). Inhibitor 41 had comparable toxicity when compared to triclosan. Inhibitors 54 and 57 were less toxic than triclosan for both cell lines. Further refinement of the chemotypes is needed to improve the therapeutic indices of these compounds.

Table 4. Cytotoxicity of Inhibitors in Neuronal and Kidney Cells (LC₅₀ Values are in μ M)

cell line	41	54	57	triclosan
786-O	7 ± 2	30 ± 10	63 ± 9	4.2 ± 0.8
Neuro2a	8 ± 2	30 ± 3	70 ± 20	5.4 ± 0.5

Effect of Inhibitors on Bacterial Growth. Inhibitors 41, 54, and 57 were tested against *F. tularensis*, *B. anthracis*, *E. coli*, *P. aeruginosa*, and *S. aureus* (Table 5). Inhibitor-41 was not

Table 5. Effects of First Round Inhibitors on Bacterial Growth (MIC Values Are in μ g/mL)

	41	54	57	ciprofloxacin	ENR enzymes
<i>F. tularensis</i> (SchuS4)	>52	22	12.9	0.125	FabI
<i>B. anthracis</i> (Ames)	>26	43	>208	0.03125	FabI
<i>E. coli</i> (25922)	>52	>343	>413	0.03125	FabI
<i>P. aeruginosa</i> (27853)	>52	>343	>413	1	FabI, FabV, FabK ^a
<i>S. aureus</i> (29213)	>52	86	>413	2	FabI

^aFabK, FabL, and FabV are resistant to triclosan.^{24,28}

effective at inhibiting bacterial growth. Inhibitor 57 was shown to inhibit the growth of *F. tularensis* SchuS4 in a species-specific manner. The measured MIC = 12.9 μ g/mL (39 μ M) was comparable to the kinetically measured K_i of 12 ± 3 μ M. It is important to note that the MIC is the concentration at which all bacterial growth is halted, while the IC₅₀ is the concentration at which 50% inhibition is observed. Here we found that the MIC and K_i were closely correlated for inhibitor 57, consistent with target-specific inhibition and minimal removal by bacterial efflux pumps.

Inhibitor **54** unexpectedly inhibited growth at concentrations twice as high as inhibitor **57** even though the measured IC_{50} values (by fluorescence and by UV-vis (Table 3)) of inhibitor **54** and **57** differed by 7-fold. Its MIC for *F. tularensis* (MIC = 22 $\mu\text{g}/\text{mL}$ (67 μM)) was comparable to that of inhibitor **57**. We believe the discrepancy arose from the low solubility of compound **54** and that the $K_i = 3.4 \pm 0.7 \mu\text{M}$ is more representative of the inhibitory activity of inhibitor **54** as the K_i was measured using lower concentrations of the inhibitor where precipitation was not observed; the compound was soluble in our in vitro assay buffer at 125 μM (Table 6). Inhibitors **54** and

Table 6. Summary of Measured IC_{50} Values in Silico Screening Hits

	no. of compds ordered	$IC_{50} < 500 \mu\text{M}$	$IC_{50} < 100 \mu\text{M}$	$IC_{50} < 20 \mu\text{M}$	interfered with assay/insoluble
round 1	75	6	4	2	28
round 2	65	13	7	2	20
total	140	19	11	4	48

57 were comparably effective in antimicrobial activity when compared to a tighter binding inhibitor ($IC_{50} = 0.3 \mu\text{M}$) previously identified and optimized by Hevener, et al.,⁷⁸ which had a MIC of 7.8 $\mu\text{g}/\text{mL}$ (26 μM).

Of the top three hits, inhibitor **54** showed a broader spectrum of growth inhibition against *F. tularensis*, *B. anthracis*, and *S. aureus* (Table 5). In contrast, **57** was species-specific. Binding mode analysis indicated that inhibitor **54** bound at the active site of FtuFabI differently from inhibitor **57**. The indole group of **54** pointed outward and interacted closely with the substrate binding loop and was adjacent to residue Arg-96. Arg-96 varied across species but was conserved in *B. anthracis* FabI; Arg-96 was replaced by a Met in *S. aureus* and a Gly in *E. coli* and *P. aeruginosa*. Because decreases in the IC_{50} values were observed for the R96G and R96M variants, we hypothesized that growth inhibition would be observed in these other bacterial species. As predicted, inhibitor **54** did inhibit bacterial growth in *F. tularensis*, *B. anthracis*, and *S. aureus*, but unexpectedly had no effect on the growth of *E. coli*. Conversely, inhibitor **57**, which had a lower IC_{50} in the R96G and R96M variants, had no effect on the growth of *B. anthracis*, *E. coli*, or *S. aureus*. Notably, these substitutions had smaller effects on the binding of inhibitor **54** when compared to the other inhibitors including triclosan. This suggests that the binding mode of the 3-substituted indole, which is predicted to differ for **54** and **57**, may be important for achieving broader spectrum inhibition; however, other mechanisms cannot be excluded.

Our MD simulations showed that the substrate binding loop was significantly stabilized upon inhibitor binding (Supporting Information Figure S5). The loop stabilization can also be seen in the greater binding free energy contributions of the loop residues in the FtuFabI-**54** binding complex when compared to the other two inhibitors (Figure 4). Therefore, the broad spectrum activity of inhibitor **54** observed in *F. tularensis*, *B. anthracis*, and *S. aureus* likely results from the well-formed loop interaction and stabilization effects in these species. Antimicrobial activity was not observed in *P. aeruginosa* likely due to the presence of FabK and FabV.^{24,28} We postulate that broad spectrum inhibition of FabIs could be achieved by targeting residues affecting loop stabilization. This may point out a new strategy for rational design of novel inhibitors of FabI with bacteriostatic activity.

Derivatives of 54 and Implications for Structure-Based Lead Optimization. To further delineate the structurally important functionalities of the chemotype of inhibitor **54**, we selected a number of its analogues and tested their inhibitory activities against *F. tularensis* FabI (Supporting Information Table S1). Replacement of the indole group with a phenyl ring significantly decreased the activity (compounds C1 and C2), indicating that the 3-substituted indole is essential to binding and inhibition. On the other hand, substitution of the phenoxy group with a phenyl ring, which was predicted to bind into the interior of the binding pocket, exhibited structure-activity relationships that were generally consistent with the binding interactions in the inner pocket. In particular, substituents at the ortho-position of the phenyl ring, such as an oxymethyl and chloride of C3 and C5, were more favorable than at the para- and meta-positions. Binding mode analysis indicated that the oxygen atom at the ortho-position formed a hydrogen-bonding interaction with Tyr-156, whereas the oxymethyl group at the para- and meta-positions more likely introduced a steric hindrance in the binding pocket. Interestingly, the indole ring with a bulky 2-substituted phenoxyethyl group (C10) showed potency comparable to inhibitor **54**. The result is also consistent with our predicted binding mode for **54**. We also tested several compounds bearing unique functionalities such as two indole groups (C14), which could potentially bind in both the interior and exterior pockets. However, compared to inhibitor **54**, these bisite inhibitors did not exhibit higher potency or broad spectrum activity (Supporting Information Tables S1 and S2). Further structure-based lead optimization such as the refinement of the linker length and removal of hydrolyzable bonds within the linker could improve the activity of these types of inhibitors.

CONCLUSION

FabI is a well validated target, and a number of chemotypes have been identified for this target to date. The two 3-substituted indole inhibitors **54** and **57** identified in this study represent novel scaffolds with low micromolar potency and antibacterial activities. Both inhibitors had lower toxicity when compared to triclosan. Owing to the unique binding properties of inhibitor **54** and **57** associated with the indole group, it is possible that a combination of the two chemotypes may better achieve high potency and bacteriostatic activity. Moreover, our MD simulation-based virtual screening protocol proved to be an efficient approach in identifying novel and potent inhibitors of FabI with bacteriostatic activity by capturing a key element of inhibitor binding in a dynamic manner. Further lead optimization and refinement of the pharmacophore could improve the chances of developing broad spectrum inhibitors of FabI as therapeutics.

ASSOCIATED CONTENT

Supporting Information

Sequence alignment of FabI enzymes from other bacteria, structures of known FabI inhibitors, bar graph of single point inhibition of the inhibitors tested, steady state kinetic analysis of FtuFabI, a general mechanism for FabI, jump dilution analysis, progress curve analysis of inhibitor **57**, and ¹H NMR and mass spectra of inhibitors **54** and **57**. This material is available free of charge via the Internet at <http://pubs.acs.org>.

AUTHOR INFORMATION

Corresponding Author

*Phone: 202-404-6037. E-mail: patricia.legler@nrl.navy.mil.
Address: 4555 Overlook Avenue, Washington, DC, United States.

Author Contributions

#X.H and J.R.C. contributed equally to this work

Notes

The authors declare no competing financial interest.

ACKNOWLEDGMENTS

We would like to acknowledge Greg Tawa for helpful discussions and Peter J. Tonge for supplying the initial plasmid DNA construct. We would also like to acknowledge Lynda Miller and Stephanie Halasohoris for excellent technical help. This work was funded by the U.S. Defense Threat Reduction Agency awards TMTI0004_09_BH_T and CBM.THERB.02.11.RD.012. The opinions or assertions contained herein belong to the authors and are not necessarily the official views of the U.S. Army, U.S. Navy or the U.S. Department of Defense.

ABBREVIATIONS USED

AMBER, assisted model building with energy refinement; ATCC, American Type Culture Collection; CAMHB, cation-adjusted Mueller–Hinton broth; CFU, colony forming unit; CrCoA, crotonyl co-enzyme A; DMSO, dimethyl sulfoxide; DOVIS, docking-based virtual screening; EDTA, ethylenediaminetetraacetic acid; FabI, fatty acid biosynthesis enzyme I; IC₅₀, half-maximal inhibitory concentration; IPTG, isopropyl β-D-1-thiogalactopyranoside; LC₅₀, half-maximal lethal concentration; LGA, Lamarckian genetic algorithm; MD, molecular dynamics; MIC, minimum inhibitory concentration; MLSMR, NIH Molecular Library Small Molecule Repository; MM/GBSA, molecular mechanics/generalized Born surface area; MM/PBSA, molecular mechanics/Poisson–Boltzmann surface area; NAD, nicotinamide adenine dinucleotide; OD, optical density; PIPES, piperazine-*N,N'*-bis(2-ethanesulfonic acid); PME, particle mesh Ewald; qHTS, quantitative high throughput screening; RMSD, root-mean-square deviation; ROCS, rapid overlay of chemical structures; SASA, solvent accessible surface area; TCL, triclosan; USP, United States Pharmacopeia; WT, wild-type

REFERENCES

- Oyston, P. C.; Griffiths, R. Francisella virulence: significant advances, ongoing challenges and unmet needs. *Expert Rev. Vaccines* **2009**, *8*, 1575–1585.
- Dennis, D. T.; Inglesby, T. V.; Henderson, D. A.; Bartlett, J. G.; Ascher, M. S.; Eitzen, E.; Fine, A. D.; Friedlander, A. M.; Hauer, J.; Layton, M.; Lillibridge, S. R.; McDade, J. E.; Osterholm, M. T.; O'Toole, T.; Parker, G.; Perl, T. M.; Russell, P. K.; Tonat, K. Tularemia as a biological weapon: medical and public health management. *JAMA, J. Am. Med. Assoc.* **2001**, *285*, 2763–2773.
- Enderlin, G.; Morales, L.; Jacobs, R. F.; Cross, J. T. Streptomycin and alternative agents for the treatment of tularemia: review of the literature. *Clin. Infect. Dis.* **1994**, *19*, 42–47.
- Selimoglu, E. Aminoglycoside-induced ototoxicity. *Curr. Pharm. Des.* **2007**, *13*, 119–126.
- Tulkens, P. M. Nephrotoxicity of aminoglycoside antibiotics. *Toxicol. Lett.* **1989**, *46*, 107–123.

- Oyston, P. C.; Sjostedt, A.; Titball, R. W. Tularemia: bioterrorism defence renews interest in *Francisella tularensis*. *Nature Rev. Microbiol.* **2004**, *2*, 967–978.

- Huth, M. E.; Ricci, A. J.; Cheng, A. G. Mechanisms of aminoglycoside ototoxicity and targets of hair cell protection. *Int. J. Otolaryngol.* **2011**, *2011*, 937861.

- Rotem, S.; Bar-Haim, E.; Cohen, H.; Elia, U.; Ber, R.; Shafferman, A.; Cohen, O. Consequences of delayed ciprofloxacin and doxycycline treatment regimens against *Francisella tularensis* airway infection. *Antimicrob. Agents Chemother.* **2012**, *56*, 5406–5408.

- Yoshida, H.; Bogaki, M.; Nakamura, M.; Nakamura, S. Quinolone resistance-determining region in the DNA gyrase *gyrA* gene of *Escherichia coli*. *Antimicrob. Agents Chemother.* **1990**, *34*, 1271–1272.

- Navas, E. Problems associated with potential massive use of antimicrobial agents as prophylaxis or therapy of a bioterrorist attack. *Clin. Microbiol. Infect.* **2002**, *8*, 534–539.

- Loveless, B. M.; Yermakova, A.; Christensen, D. R.; Kondig, J. P.; Heine, H. S., III; Wasielewski, L. P.; Kulesh, D. A. Identification of ciprofloxacin resistance by SimpleProbe, High Resolution Melt and Pyrosequencing nucleic acid analysis in biothreat agents: *Bacillus anthracis*, *Yersinia pestis* and *Francisella tularensis*. *Mol. Cell Probes* **2010**, *24*, 154–160.

- Price, L. B.; Vogler, A.; Pearson, T.; Busch, J. D.; Schupp, J. M.; Keim, P. In vitro selection and characterization of *Bacillus anthracis* mutants with high-level resistance to ciprofloxacin. *Antimicrob. Agents Chemother.* **2003**, *47*, 2362–2365.

- Lindler, L. E.; Fan, W.; Jahan, N. Detection of ciprofloxacin-resistant *Yersinia pestis* by fluorogenic PCR using the LightCycler. *J. Clin. Microbiol.* **2001**, *39*, 3649–3655.

- Yoshida, H.; Bogaki, M.; Nakamura, M.; Yamanaka, L. M.; Nakamura, S. Quinolone resistance-determining region in the DNA gyrase *gyrB* gene of *Escherichia coli*. *Antimicrob. Agents Chemother.* **1991**, *35*, 1647–1650.

- Ho, P. L.; Yung, R. W.; Tsang, D. N.; Que, T. L.; Ho, M.; Seto, W. H.; Ng, T. K.; Yam, W. C.; Ng, W. W. Increasing resistance of *Streptococcus pneumoniae* to fluoroquinolones: results of a Hong Kong multicentre study in 2000. *J. Antimicrob. Chemother.* **2001**, *48*, 659–665.

- Johnson, A. P.; Sheppard, C. L.; Harnett, S. J.; Birtles, A.; Harrison, T. G.; Brenwald, N. P.; Gill, M. J.; Walker, R. A.; Livermore, D. M.; George, R. C. Emergence of a fluoroquinolone-resistant strain of *Streptococcus pneumoniae* in England. *J. Antimicrob. Chemother.* **2003**, *52*, 953–960.

- Huang, S. S.; Labus, B. J.; Samuel, M. C.; Wan, D. T.; Reingold, A. L. Antibiotic resistance patterns of bacterial isolates from blood in San Francisco County, California, 1996–1999. *Emerg. Infect. Dis.* **2002**, *8*, 195–201.

- The Surveillance Network, 2009.

- Lu, H.; England, K.; am, E. C.; Truglio, J. J.; Luckner, S.; Reddy, B. G.; Marlenee, N. L.; Knudson, S. E.; Knudson, D. L.; Bowen, R. A.; Kisker, C.; Slayden, R. A.; Tonge, P. J. Slow-onset inhibition of the FabI enoyl reductase from *Francisella tularensis*: residence time and in vivo activity. *ACS Chem. Biol.* **2009**, *4*, 221–231.

- Wen, L.; Chmielowski, J. N.; Bohn, K. C.; Huang, J. K.; Timsina, Y. N.; Kodali, P.; Pathak, A. K. Functional expression of *Francisella tularensis* FabH and FabI, potential antibacterial targets. *Protein Express. Purif.* **2009**, *65*, 83–91.

- Heath, R. J.; Su, N.; Murphy, C. K.; Rock, C. O. The enoyl-[acyl-carrier-protein] reductases FabI and FabL from *Bacillus subtilis*. *J. Biol. Chem.* **2000**, *275*, 40128–40133.

- Marrakchi, H.; Dewolf, W. E., Jr.; Quinn, C.; West, J.; Polizzi, B. J.; So, C. Y.; Holmes, D. J.; Reed, S. L.; Heath, R. J.; Payne, D. J.; Rock, C. O.; Wallis, N. G. Characterization of *Streptococcus pneumoniae* enoyl-(acyl-carrier protein) reductase (FabK). *Biochem. J.* **2003**, *370*, 1055–1062.

- Kim, K. H.; Ha, B. H.; Kim, S. J.; Hong, S. K.; Hwang, K. Y.; Kim, E. E. Crystal structures of Enoyl-ACP reductases I (FabI) and III (FabL) from *B. subtilis*. *J. Mol. Biol.* **2011**, *406*, 403–415.

- (24) Heath, R. J.; Rock, C. O. A triclosan-resistant bacterial enzyme. *Nature* **2000**, *406*, 145–146.
- (25) Kim, K. H.; Ha, B. H.; Kim, S. J.; Hong, S. K.; Hwang, K. Y.; Kim, E. E. Crystal structures of Enoyl-ACP reductases I (FabI) and III (FabL) from *B. subtilis*. *J. Mol. Biol.* **2011**, *406*, 403–415.
- (26) Park, A. K.; Lee, J. H.; Chi, Y. M.; Moon, J. H. Crystallization and preliminary X-ray crystallographic studies of a new class of enoyl-(acyl-carrier protein) reductase, FabV, from *Vibrio fischeri*. *Acta Crystallogr., Sect. F: Struct. Biol. Cryst. Commun.* **2012**, *68*, 78–80.
- (27) Massengo-Tiasse, R. P.; Cronan, J. E. *Vibrio cholerae* FabV defines a new class of enoyl-acyl carrier protein reductase. *J. Biol. Chem.* **2008**, *283*, 1308–1316.
- (28) Zhu, L.; Lin, J.; Ma, J.; Cronan, J. E.; Wang, H. Triclosan resistance of *Pseudomonas aeruginosa* PAO1 is due to FabV, a triclosan-resistant enoyl-acyl carrier protein reductase. *Antimicrob. Agents Chemother.* **2010**, *54*, 689–698.
- (29) Hirschbeck, M. W.; Kuper, J.; Lu, H.; Liu, N.; Neckles, C.; Shah, S.; Wagner, S.; Sottriffer, C. A.; Tonge, P. J.; Kisker, C. Structure of the *Yersinia pestis* FabV enoyl-ACP reductase and its interaction with two 2-pyridone inhibitors. *Structure* **2012**, *20*, 89–100.
- (30) Lu, H.; Tonge, P. J. Mechanism and inhibition of the FabV enoyl-ACP reductase from *Burkholderia mallei*. *Biochemistry* **2010**, *49*, 1281–1289.
- (31) Kingry, L. C.; Cummings, J. E.; Brookman, K. W.; Bommineni, G. R.; Tonge, P. J.; Slayden, R. A. The *Francisella tularensis* FabI enoyl-acyl carrier protein reductase gene is essential to bacterial viability and is expressed during infection. *J. Bacteriol.* **2013**, *195*, 351–358.
- (32) Balemans, W.; Lounis, N.; Gilissen, R.; Guillemont, J.; Simmen, K.; Andries, K.; Koul, A. Essentiality of FASII pathway for *Staphylococcus aureus*. *Nature* **2010**, *463*, E3.
- (33) Kaplan, N.; Awrey, D.; Bardouniotis, E.; Berman, J.; Yethon, J.; Pauls, H. W.; Hafkin, B. In vitro activity (MICs and rate of kill) of AFN-1252, a novel FabI inhibitor, in the presence of serum and in combination with other antibiotics. *J. Chemother.* **2013**, *25*, 18–25.
- (34) Karlowsky, J. A.; Laing, N. M.; Baudry, T.; Kaplan, N.; Vaughan, D.; Hoban, D. J.; Zhan, G. G. In vitro activity of API-1252, a novel FabI inhibitor, against clinical isolates of *Staphylococcus aureus* and *Staphylococcus epidermidis*. *Antimicrob. Agents Chemother.* **2007**, *51*, 1580–1581.
- (35) England, K.; Am, E. C.; Lu, H.; Sullivan, T. J.; Marlenee, N. L.; Bowen, R. A.; Knudson, S. E.; Knudson, D. L.; Tonge, P. J.; Slayden, R. A. Substituted diphenyl ethers as a broad-spectrum platform for the development of chemotherapeutics for the treatment of tularaemia. *J. Antimicrob. Chemother.* **2009**, *64*, 1052–1061.
- (36) Sivaraman, S.; Zwahlen, J.; Bell, A. F.; Hedstrom, L.; Tonge, P. J. Structure–activity studies of the inhibition of FabI, the enoyl reductase from *Escherichia coli*, by triclosan: kinetic analysis of mutant FabIs. *Biochemistry* **2003**, *42*, 4406–4413.
- (37) McMurry, L. M.; Oethinger, M.; Levy, S. B. Triclosan targets lipid synthesis. *Nature* **1998**, *394*, 531–532.
- (38) Wu, J. L.; Liu, J.; Cai, Z. Determination of triclosan metabolites by using in-source fragmentation from high-performance liquid chromatography/negative atmospheric pressure chemical ionization ion trap mass spectrometry. *Rapid Commun. Mass Spectrom.* **2010**, *24*, 1828–1834.
- (39) Silver, L. L. Challenges of antibacterial discovery. *Clin. Microbiol. Rev.* **2011**, *24*, 71–109.
- (40) Kim, K. H.; Ha, B. H.; Kim, S. J.; Hong, S. K.; Hwang, K. Y.; Kim, E. E. Crystal structures of enoyl-ACP reductases I (FabI) and III (FabL) from *B. subtilis*. *J. Mol. Biol.* **2011**, *406*, 403–415.
- (41) Rafi, S.; Novichenok, P.; Kolappan, S.; Zhang, X.; Stratton, C. F.; Rawat, R.; Kisker, C.; Simmerling, C.; Tonge, P. J. Structure of acyl carrier protein bound to FabI, the FASII enoyl reductase from *Escherichia coli*. *J. Biol. Chem.* **2006**, *281*, 39285–39293.
- (42) Rafi, S. B.; Cui, G.; Song, K.; Cheng, X.; Tonge, P. J.; Simmerling, C. Insight through molecular mechanics Poisson–Boltzmann surface area calculations into the binding affinity of triclosan and three analogues for FabI, the *E. coli* enoyl reductase. *J. Med. Chem.* **2006**, *49*, 4574–4580.
- (43) Lu, H.; Tonge, P. J. Inhibitors of FabI, an enzyme drug target in the bacterial fatty acid biosynthesis pathway. *Acc. Chem. Res.* **2008**, *41*, 11–20.
- (44) Mehboob, S.; Truong, K.; Santarsiero, B. D.; Johnson, M. E. Structure of the *Francisella tularensis* enoyl-acyl carrier protein reductase (FabI) in complex with NAD(+) and triclosan. *Acta Crystallogr., Sect. F: Struct. Biol. Cryst. Commun.* **2010**, *66*, 1436–1440.
- (45) Stewart, M. J.; Parikh, S.; Xiao, G.; Tonge, P. J.; Kisker, C. Structural basis and mechanism of enoyl reductase inhibition by triclosan. *J. Mol. Biol.* **1999**, *290*, 859–865.
- (46) Okimoto, N.; Futatsugi, N.; Fuji, H.; Suenaga, A.; Morimoto, G.; Yanai, R.; Ohno, Y.; Narumi, T.; Taiji, M. High-performance drug discovery: computational screening by combining docking and molecular dynamics simulations. *PLoS. Comput. Biol.* **2009**, *5*, e1000528.
- (47) Ward, W. H.; Holdgate, G. A.; Rowsell, S.; McLean, E. G.; Pauptit, R. A.; Clayton, E.; Nichols, W. W.; Colls, J. G.; Minshull, C. A.; Jude, D. A.; Mistry, A.; Timms, D.; Camble, R.; Hales, N. J.; Britton, C. J.; Taylor, I. W. Kinetic and structural characteristics of the inhibition of enoyl (acyl carrier protein) reductase by triclosan. *Biochemistry* **1999**, *38*, 12514–12525.
- (48) *Methods for Dilution Antimicrobial Susceptibility Tests for Bacteria That Grow Aerobically*; Approved Standard M07-A7; Clinical and Laboratory Standards Institute: Wayne, PA, 2006.
- (49) Mehboob, S.; Truong, K.; Santarsiero, B. D.; Johnson, M. E. Structure of the *Francisella tularensis* enoyl-acyl carrier protein reductase (FabI) in complex with NAD(+) and triclosan. *Acta Crystallogr., Sect. F: Struct. Biol. Cryst. Commun.* **2010**, *66*, 1436–1440.
- (50) Sali, A.; Blundell, T. L. Comparative protein modelling by satisfaction of spatial restraints. *J. Mol. Biol.* **1993**, *234*, 779–815.
- (51) Jiang, X.; Kumar, K.; Hu, X.; Wallqvist, A.; Reifman, J. DOVIS 2.0: an efficient and easy to use parallel virtual screening tool based on AutoDock 4.0. *Chem. Cent. J.* **2008**, *2*, 18.
- (52) Zhang, S.; Kumar, K.; Jiang, X.; Wallqvist, A.; Reifman, J. DOVIS: an implementation for high-throughput virtual screening using AutoDock. *BMC Bioinform.* **2008**, *9*, 126.
- (53) Freundlich, J. S.; Wang, F.; Tsai, H. C.; Kuo, M.; Shieh, H. M.; Anderson, J. W.; Nkrumah, L. J.; Valderramos, J. C.; Yu, M.; Kumar, T. R.; Valderramos, S. G.; Jacobs, W. R., Jr.; Schiehsler, G. A.; Jacobus, D. P.; Fidock, D. A.; Sacchettini, J. C. X-ray structural analysis of *Plasmodium falciparum* enoyl acyl carrier protein reductase as a pathway toward the optimization of triclosan antimalarial efficacy. *J. Biol. Chem.* **2007**, *282*, 25436–25444.
- (54) Kim, K. H.; Ha, B. H.; Kim, S. J.; Hong, S. K.; Hwang, K. Y.; Kim, E. E. Crystal structures of enoyl-ACP reductases I (FabI) and III (FabL) from *B. subtilis*. *J. Mol. Biol.* **2011**, *406*, 403–415.
- (55) Heerding, D. A.; Chan, G.; DeWolf, W. E.; Fosberry, A. P.; Janson, C. A.; Jaworski, D. D.; McManus, E.; Miller, W. H.; Moore, T. D.; Payne, D. J.; Qiu, X.; Rittenhouse, S. F.; Slater-Radosti, C.; Smith, W.; Takata, D. T.; Vaidya, K. S.; Yuan, C. C.; Huffman, W. F. 1,4-Disubstituted imidazoles are potential antibacterial agents functioning as inhibitors of enoyl acyl carrier protein reductase (FabI). *Bioorg. Med. Chem. Lett.* **2001**, *11*, 2061–2065.
- (56) Miller, W. H.; Seefeld, M. A.; Newlander, K. A.; Uzinskas, I. N.; Burgess, W. J.; Heerding, D. A.; Yuan, C. C.; Head, M. S.; Payne, D. J.; Rittenhouse, S. F.; Moore, T. D.; Pearson, S. C.; Berry, V.; Dewolf, W. E., Jr.; Keller, P. M.; Polizzi, B. J.; Qiu, X.; Janson, C. A.; Huffman, W. F. Discovery of aminopyridine-based inhibitors of bacterial enoyl-ACP reductase (FabI). *J. Med. Chem.* **2002**, *45*, 3246–3256.
- (57) Seefeld, M. A.; Miller, W. H.; Newlander, K. A.; Burgess, W. J.; DeWolf, W. E., Jr.; Elkins, P. A.; Head, M. S.; Jakas, D. R.; Janson, C. A.; Keller, P. M.; Manley, P. J.; Moore, T. D.; Payne, D. J.; Pearson, S.; Polizzi, B. J.; Qiu, X.; Rittenhouse, S. F.; Uzinskas, I. N.; Wallis, N. G.; Huffman, W. F. Indole naphthyridinones as inhibitors of bacterial enoyl-ACP reductases FabI and FabK. *J. Med. Chem.* **2003**, *46*, 1627–1635.
- (58) Wishart, D. S.; Knox, C.; Guo, A. C.; Shrivastava, S.; Hassanali, M.; Stothard, P.; Chang, Z.; Woolsey, J. DrugBank: a comprehensive

resource for in silico drug discovery and exploration. *Nucleic Acids Res.* **2006**, *34*, D668–D672.

(59) Rush, T. S., III; Grant, J. A.; Mosyak, L.; Nicholls, A. A shape-based 3-D scaffold hopping method and its application to a bacterial protein–protein interaction. *J. Med. Chem.* **2005**, *48*, 1489–1495.

(60) Case, D. A.; Cheatham, T. E., III; Darden, T.; Gohlke, H.; Luo, R.; Merz, K. M., Jr.; Onufriev, A.; Simmerling, C.; Wang, B.; Woods, R. J. The Amber biomolecular simulation programs. *J. Comput. Chem.* **2005**, *26*, 1668–1688.

(61) Darden, T.; York, D.; Pedersen, L. Particle mesh Ewald: an $N \log(N)$ method for Ewald sums in large systems. *J. Chem. Phys.* **1993**, *98*, 10089–10092.

(62) Berendsen, H. J.; Postma, J. P.; van Gunsteren, W. F.; Dinola, A.; Haak, J. R. Molecular dynamics with coupling to an external bath. *J. Chem. Phys.* **1984**, *81*, 3684–3690.

(63) Kollman, P. A.; Massova, I.; Reyes, C.; Kuhn, B.; Huo, S.; Chong, L.; Lee, M.; Lee, T.; Duan, Y.; Wang, W.; Donini, O.; Cieplak, P.; Srinivasan, J.; Case, D. A.; Cheatham, T. E., III. Calculating structures and free energies of complex molecules: combining molecular mechanics and continuum models. *Acc. Chem. Res.* **2000**, *33*, 889–897.

(64) Lee, H. H.; Moon, J.; Suh, S. W. Crystal structure of the *Helicobacter pylori* enoyl-acyl carrier protein reductase in complex with hydroxydiphenyl ether compounds, triclosan and diclosan. *Proteins* **2007**, *69*, 691–694.

(65) Tipparaju, S. K.; Mulhearn, D. C.; Klein, G. M.; Chen, Y.; Tapadar, S.; Bishop, M. H.; Yang, S.; Chen, J.; Ghassemi, M.; Santarsiero, B. D.; Cook, J. L.; Johlfs, M.; Mesecar, A. D.; Johnson, M. E.; Kozikowski, A. P. Design and synthesis of aryl ether inhibitors of the *Bacillus anthracis* enoyl-ACP reductase. *ChemMedChem.* **2008**, *3*, 1250–1268.

(66) Miron, S.; Munier-Lehmann, H.; Craescu, C. T. Structural and dynamic studies on ligand-free adenylate kinase from *Mycobacterium tuberculosis* revealed a closed conformation that can be related to the reduced catalytic activity. *Biochemistry* **2004**, *43*, 67–77.

(67) Perozzo, R.; Kuo, M.; Sidhu, A.; Valiyaveetil, J. T.; Bittman, R.; Jacobs, W. R., Jr.; Fidock, D. A.; Sacchettini, J. C. Structural elucidation of the specificity of the antibacterial agent triclosan for malarial enoyl acyl carrier protein reductase. *J. Biol. Chem.* **2002**, *277*, 13106–13114.

(68) Heath, R. J.; Rubin, J. R.; Holland, D. R.; Zhang, E.; Snow, M. E.; Rock, C. O. Mechanism of triclosan inhibition of bacterial fatty acid synthesis. *J. Biol. Chem.* **1999**, *274*, 11110–11114.

(69) Sivaraman, S.; Sullivan, T. J.; Johnson, F.; Novichenok, P.; Cui, G.; Simmerling, C.; Tonge, P. J. Inhibition of the bacterial enoyl reductase FabI by triclosan: a structure–reactivity analysis of FabI inhibition by triclosan analogues. *J. Med. Chem.* **2004**, *47*, 509–518.

(70) Parikh, S. L.; Xiao, G.; Tonge, P. J. Inhibition of InhA, the enoyl reductase from *Mycobacterium tuberculosis*, by triclosan and isoniazid. *Biochemistry* **2000**, *39*, 7645–7650.

(71) Payne, D. J.; Miller, W. H.; Berry, V.; Brosky, J.; Burgess, W. J.; Chen, E.; DeWolf, J. W., Jr.; Fosberry, A. P.; Greenwood, R.; Head, M. S.; Heerding, D. A.; Janson, C. A.; Jaworski, D. D.; Keller, P. M.; Manley, P. J.; Moore, T. D.; Newlander, K. A.; Pearson, S.; Polizzi, B. J.; Qiu, X.; Rittenhouse, S. F.; Slater-Radosti, C.; Salyers, K. L.; Seefeld, M. A.; Smyth, M. G.; Takata, D. T.; Uzinskas, I. N.; Vaidya, K.; Wallis, N. G.; Winram, S. B.; Yuan, C. C.; Huffman, W. F. Discovery of a novel and potent class of FabI-directed antibacterial agents. *Antimicrob. Agents Chemother.* **2002**, *46*, 3118–3124.

(72) Fawcett, T.; Copse, C. L.; Simon, J. W.; Slabas, A. R. Kinetic mechanism of NADH-enoyl-ACP reductase from *Brassica napus*. *FEBS Lett.* **2000**, *484*, 65–68.

(73) Marcinkeviciene, J.; Jiang, W.; Kopcho, L. M.; Locke, G.; Luo, Y.; Copeland, R. A. Enoyl-ACP reductase (FabI) of *Haemophilus influenzae*: steady-state kinetic mechanism and inhibition by triclosan and hexachlorophene. *Arch. Biochem. Biophys.* **2001**, *390*, 101–108.

(74) de Medeiros, P. S.; Ducati, R. G.; Basso, L. A.; Santos, D. S.; da Silva, L. H. Enzyme Mechanism and Slow-Onset Inhibition of *Plasmodium falciparum* Enoyl-Acyl Carrier Protein Reductase by an Inorganic Complex. *Enzyme Res.* **2011**, *2011*, 642758.

(75) Yu, B. J.; Kim, J. A.; Pan, J. G. Signature gene expression profile of triclosan-resistant *Escherichia coli*. *J. Antimicrob. Chemother.* **2010**, *65*, 1171–1177.

(76) Xu, H.; Sullivan, T. J.; Sekiguchi, J.; Kirikae, T.; Ojima, I.; Stratton, C. F.; Mao, W.; Rock, F. L.; Alley, M. R.; Johnson, F.; Walker, S. G.; Tonge, P. J. Mechanism and inhibition of saFabI, the enoyl reductase from *Staphylococcus aureus*. *Biochemistry* **2008**, *47*, 4228–4236.

(77) Leskovac, V. Kinetics of Rapid Equilibrium Bisubstrate Reactions. In *Comprehensive Enzyme Kinetics*; Kluwer Academic Publishers: New York, 2004; Chapter 8, pp 117–138.

(78) Hevener, K. E.; Mehboob, S.; Su, P. C.; Truong, K.; Boci, T.; Deng, J.; Ghassemi, M.; Cook, J. L.; Johnson, M. E. Discovery of a novel and potent class of *F. tularensis* enoyl-reductase (FabI) inhibitors by molecular shape and electrostatic matching. *J. Med. Chem.* **2012**, *55*, 268–279.